Control of Systems With Hysteresis via Servocompensation and Its Application to Nanopositioning

Alex Esbrook, *Student Member, IEEE*, Xiaobo Tan, *Senior Member, IEEE*, and Hassan K. Khalil, *Fellow, IEEE*

Abstract—Partly motivated by nanopositioning applications in scanning probe microscopy systems, we consider the problem of tracking periodic signals for a class of systems consisting of linear dynamics preceded by a hysteresis operator, where uncertainties exist in both the dynamics and the hysteresis. A robustified servocompensator is proposed, in combination with an approximate hysteresis inverse, to achieve high-precision tracking. The servocompensator accommodates the internal model of the reference signal and a finite number of harmonic terms. Using a Prandtl–Ishlinskii (PI) operator for modeling hysteresis, we show that the closed-loop system admits a unique and asymptotically stable periodic solution, which justifies treating the inversion error as an exogenous periodic disturbance. Consequently, the asymptotic tracking error can be made arbitrarily small as the servocompensator accommodates a sufficient number of harmonic terms. The analysis is further extended to the case where the hysteresis is modeled by a modified PI operator. Experiments on a commercial nanopositioner show that, with the proposed method, tracking can be achieved for a 200-Hz reference signal with 0.52% mean error and 1.5% peak error, for a travel range of 40 μm. The performance of the proposed method in tracking both sinusoidal and sawtooth signals does not fall off with increasing frequency as fast as the proportional-integral controller and the iterative learning controller, both adopted in this paper for comparison purposes. Further, the proposed controller shows excellent robustness to loading conditions.

Index Terms—Hysteresis, nanopositioning control, piezoelectrics, servocompensator, tracking.

I. INTRODUCTION

NANOPOSITIONING plays a key role in advanced technologies, such as scanning probe microscopy (SPM), ultra-high density data storage, and micro/nanofabrication [1]. In SPM, a sample to be measured or manipulated is moved beneath a sharp tip with nanometer precision, commonly through piezoelectric actuators. Consequently, the imaging or manipulation speed of an SPM system is closely tied to the performance of the piezo-based nanopositioner. Precision control of piezo-actuated systems is complicated by the strong coupling between the hysteresis nonlinearity and the vibration dynamics [1]. In addition, both the hysteresis and the dynamics can vary with the environmental or loading conditions. However, the high actuation speed and fine resolution of piezoelectric materials have made them the preferred actuator for nanopositioning, and have motivated significant interest in control design to combat their shortcomings [1].

Modeling and control of hysteretic systems have received much attention in the literature [2]. Hysteresis models can be roughly classified as physics-based or phenomenology-based. A notable example of a physics-based model is the ferromagnetic hysteresis model proposed by Jiles and Atherton [3]. Formulated in terms of switching differential equations, the latter model belongs to the class of Duhem hysteresis models [4], [5]. Starting in early 1970s, systematic studies on hysteresis were conducted by Krasnoselskii, Pokrovskii, and others, who examined rate-independent hysteresis operators constructed out of elementary hysteresis units called hysterons [6]. Examples of such operators, include the Preisach operator [7], the Prandtl–Ishlinskii (PI) operator, and the Krasnoselskii–Porkovskii (KP) operator among others. Generally independent from specific physical systems, these operators can serve as phenomenological models for a large class of hysteretic systems. Further developments by Mayergoyz [8], Visintin [4], Brokate and Sprekels [9], and Krejci [10] in the 1980s led to an understanding of general hysteresis operators, and ordinary differential equations (ODEs) and partial differential equations coupled with hysteresis operators.

Hysteresis modeling continued to receive great interest in the 1990s and beyond, which, to a large extent, was due to the advances made in various smart materials (piezoelectrics, magnetostrictives, shape memory alloys, and etc.) and devices and systems driven by these materials [11]. These materials typically possess multiple stable equilibria for a given input and thus exhibit hysteresis behavior. The interest in smart material-actuated systems also spurred the development of control methods for hysteretic systems. In modeling piezo-actuated nanopositioners and many other smart material-actuated systems, a reasonable model structure is a linear dynamical system preceded by a hysteresis module [1], [12]–[15]. While qualitative properties of hysteresis models, such as the passivity (defined properly) of the Preisach operator, can be used for control analysis and synthesis [16], a predominant class of control approaches involve approximate cancellation of the hysteresis effect through inversion [12], [17], which is illustrated in Fig. 1.
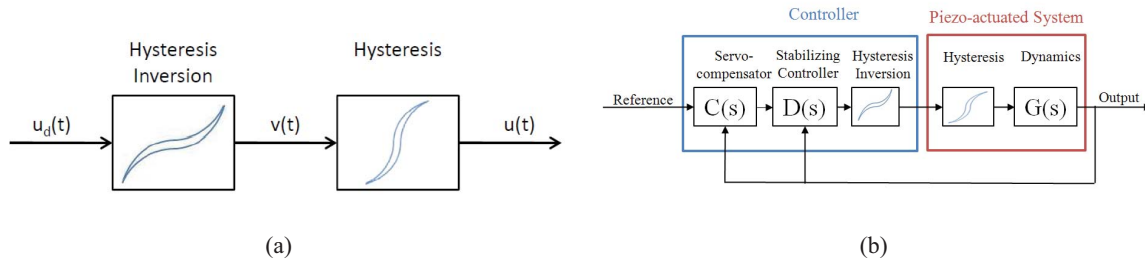
Fig. 1.   (a) Illustration of the feed-forward hysteresis inversion process. (b) Proposed controller structure: a servocompensator/stabilizing controller followed by an approximate inverse compensator for hysteresis.

Hysteresis inversion has been studied for a number of operators. For example, the inverse of a Preisach operator, which does not admit an analytical form, has been constructed approximately through data-intensive table-lookup based on the so called Everett function [8], [18], using a Preisach-based pseudo-compensator identified with reversed input–output data [13], [19], [20], and through an iterative procedure that is based on the piecewise monotonicity of the Preisach operator [21]–[23]. On the other hand, analytical formulas exist for the inverse of finite-dimensional classical [24], modified [25], and generalized [26] PI operators. Inversion has also been investigated for other hysteresis operators, such as a KP operator [27] and a homogenized energy model [28].

Feedback control is often used in combination with hysteresis inverse to mitigate the effect of inversion error and to deal with the remaining dynamics of the system [21], [22], [29]. One important source of inversion error is the uncertainty in hysteresis parameters, for which adaptive control offers a potentially effective solution. Adaptive inverse control was studied for a PI operator by Kuhnen and Janocha [30], and for a Preisach operator by Tan and Baras [31]. In [17] and [32], uncertainties in both the plant dynamics and hysteresis model are addressed with model-reference adaptive inverse control. Adaptive control has also been proposed for uncertain discrete-time systems with hysteresis [14].

In the piezo-based micro/nanopositioning literature, the effect of hysteresis or inversion error is often considered to be an unknown disturbance, and various control techniques are used to reduce the effect of this disturbance on system performance. The industry standard in control of nanopositioning systems has been proportional-integral (P+I) control. However, a P+I controller is not capable of tracking at high frequency without possibly destabilizing the system [33]. Recently, several robust control methods have also been proposed that do not make use of an explicit hysteresis models [34], [35]. High-gain feedback together with a notch-filter was proposed to linearize hysteresis by Zou et al. [36]. In [37], the hysteresis is approximated by a straight line, and an adaptive robust controller is then used to handle the uncertainties, including the hysteresis effect. Sliding mode control has been used to achieve robustness to system uncertainties [33]. Disturbance observers are also gaining popularity for use in estimating disturbances caused by hysteresis [38].

In this paper, we consider the problem of tracking periodic signals for a class of systems consisting of linear dynamics preceded by a hysteresis operator, where uncertainties exist in both the dynamics and the hysteresis. This problem is partly motivated by the nanopositioning applications in SPM systems, where the sample being scanned is typically moved periodically by a piezo actuator. As illustrated in Fig. 1, we propose the use of a servocompensator [39], [40] in combination with an approximate hysteresis inverse based on the PI operator to achieve high-precision tracking. This operator and its generalized versions have proven effective in modeling piezoelectric hysteresis [14], [25], [41], [42]. It also possesses a contraction property [32], which is vital to our work. In addition, the inverse of a PI operator with a finite number of hysterons can be constructed explicitly [25]; therefore, it is well suited for online implementation. For the ease of presentation, we will focus the discussion on the case involving the classical PI operator. But we will also extend the results to the case involving a modified PI operator [25], which is adopted in the nanopositioning experiments reported later in this paper.

To motivate the use of servocompensators for control of such systems, we present Fig. 2, which shows the spectrum of the inversion error resulting from approximate inversion of a modified PI operator [25], when a sinusoid of 5 Hz is applied to the input of the inverse operator. Here, the imperfect inversion is due to the mismatch between the weight parameters of the hysteresis operator based upon which the inverse is constructed and those of the forward hysteresis operator. From Fig. 2, it can be seen that the inversion error consists of harmonics of the input signal applied to the inverse operator, where the first few harmonics dominate the spectrum. It is shown in this paper that, under appropriate conditions, with a classical or modified PI operator modeling the hysteresis, the closed-loop system admits a unique, asymptotically stable, periodic solution. The latter implies that, with a periodic reference signal, the input to the inverse hysteresis operator is indeed asymptotically periodic, which justifies treating the inversion error as an exogenous, periodic disturbance that consists of harmonics of the reference input. The properties of servocompensators guarantee that any periodic disturbance whose generating model is contained in the internal model of the controller will be canceled out at the steady state. Consequently, the asymptotic tracking error can be made arbitrarily small when the servocompensator accommodates a sufficient number of harmonic terms. We will refer to this design as a multiharmonic servocompensator (MHSC).
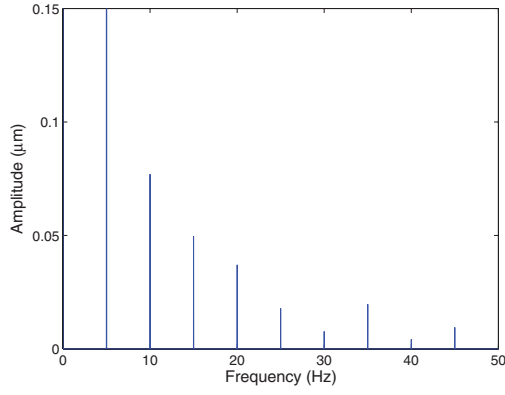
Fig. 2. Spectrum of typical inversion error $u_d - u$ for a modified PI operator, generated by a sinusoidal input. The first harmonic is much larger than shown on this figure.

The proposed method only requires an approximate model of the hysteresis. Robustness with respect to uncertainties in the dynamics is also established using results from [43]. Therefore, our design approach addresses the uncertainties in both hysteresis and dynamics. Comparing to the adaptive approaches [17], [32], our method requires much less online computation. It also differs from many others in the literature in that we exploit the specific effect hysteresis has on our system at the steady-state, rather than simply treating it as an unknown disturbance.

We compare the proposed method with iterative learning control (ILC) [15] and proportional–integral (P+I) control combined with hysteresis inversion. ILC is considered a competitive approach in nanopositioning, and it has shown great promise in tracking periodic signals, with high tracking bandwidth and performance. Experiments on a nanopositioner have confirmed the effectiveness of our proposed control scheme. In particular, we have demonstrated tracking of a 200-Hz reference signal with 0.52% mean error and 1.57% peak error for a travel range of 40 μm, compared with 1.31% mean and 3.2% peak errors, respectively, for ILC. Investigations into the robustness of the proposed method against different loading conditions have shown that the mean tracking error increases only 1.4% relative to the unloaded case, for a load of 40% of the maximum mass recommended by the manufacturer, as compared to an 18.5% increase for ILC. Experimental results have also shown that the performance of the proposed method drops much slower with increasing frequency than those of the ILC and P+I methods.

The remainder of this paper is organized as follows. Linear servocompensator theory is first reviewed in Section II, where we also present our design of the stabilizing controller. Hysteresis modeling and inversion are then discussed in Section III, where we further establish the existence and asymptotic stability of periodic solutions of the closed-loop system, when a classical PI operator is involved and state feedback control is used. In Section IV, we extend the results to consider a modified PI operator and output feedback control where a Luenberger observer is adopted to estimate the state. Experimental results are presented and discussed in Section V.

Finally, concluding remarks are provided in Section VI. Some preliminary results in this paper were presented in [44].

II. LINEAR SERVOCOMPENSATOR THEORY AND CONTROLLER DESIGN

Recall Fig. 1(a) and (b). As we will show in Section III-B, under suitable conditions, the combined effect of the approximate inverse hysteresis model and the hysteresis model can be treated as an exogenous disturbance to the linear dynamics. Note that, for a reasonably large range of inputs, the dynamics of a piezo-actuated SPM system (excluding the hysteresis part) can be treated as linear [13], [34]. In this section, we review the servocompensator theory and design a robustly stabilizing controller for a linear system.

Servocompensators, based on the internal model principle, were developed in the 1970s by Davison [39] and Francis [40]. The underlying principle used by servocompensators is that they are dynamic oscillators, which allows them to generate a control signal without being driven by an input. In particular, Davison and Francis proved that for linear systems, a servocompensator can regulate a tracking error to zero, if the internal model of the signal to be tracked is contained within the servocompensator. Consider a linear system given by

$$\dot{x}(t) = Ax(t) + Bu(t) + Ew(t)$$
$$e(t) = y_r(t) - Cx(t) - Du(t) \qquad (1)$$

where $x \in \mathbb{R}^n$ is the plant state, $u \in \mathbb{R}$ is the plant input, $y = Cx + Du$ is the plant output, $e \in \mathbb{R}$ is the tracking error, $w = H\sigma \in \mathbb{R}^{p \times 1}$ is an exogenous disturbance, and $y_r = G\sigma \in \mathbb{R}$ is the reference trajectory to be tracked. Here H and G are real matrices, which map the vector $\sigma \in \mathbb{R}^p$ to $\mathbb{R}^p$ and $\mathbb{R}$, respectively. The vector σ is generated by a linear exosystem

$$\dot{\sigma}(t) = S\sigma(t) \qquad (2)$$

where $S \in \mathbb{R}^{p \times p}$. $E \in \mathbb{R}^{n \times p}$ translates the disturbance w from the exosystem to the plant. Denote by eig(S), the set of distinct eigenvalues of the matrix S. It is assumed that (A, B, C, D) is a minimal realization of a SISO plant transfer function, and thus is controllable and observable. The following assumptions are made on the system.

Assumption 1: eig(S) $\subset$ clos($\mathbf{C}^+$) $\triangleq \{\lambda \in \mathbf{C}, \ Re[\lambda] \geq 0\}$.

Assumption 2: The system (A, B, C, D) has no zeros in eig(S).

Remark 1: In order to simplify the presentation, we will assume for the remainder of our work that the matrix $D = 0$. This assumption is satisfied, in particular, for the nanopositioning plant used in our experimental work.

The controller is designed as

$$\dot{\eta}(t) = \mathbf{C}^* \eta(t) + \mathbf{B}^* e(t) \qquad (3)$$
$$u(t) = -K_1 x(t) - K_2 \eta(t) \qquad (4)$$

where $\mathbf{C}^* \in \mathbb{R}^{p \times p}$ has the same eigenvalues as those of S. $\mathbf{B}^*$ is chosen such that the pair $(\mathbf{C}^*, \mathbf{B}^*)$ is controllable. By [45, Th. 1] if the gain matrices (K_1, K_2) can be chosen such that the resulting closed-loop matrix is Hurwitz, then $e(t) \to 0$ as $t \to \infty$. It is shown in [46] that a necessary and sufficient

condition for solvability of this problem is that there exist matrices $\Pi \in \mathbb{R}^{n \times p}$ and $\Gamma \in \mathbb{R}^{1 \times p}$, which solve the linear matrix equations

$$\Pi S = A\Pi + B\Gamma + E \qquad C\Pi = 0. \qquad (5)$$

Adding the servocompensator (3) to the linear plant (1), the system becomes

$$\begin{bmatrix} \dot{x}(t) \\ \dot{\eta}(t) \end{bmatrix} = \begin{bmatrix} A & 0 \\ -\mathbf{B}^*C & \mathbf{C}^* \end{bmatrix} \begin{bmatrix} x(t) \\ \eta(t) \end{bmatrix} + \begin{bmatrix} Bu(t) + Ew(t) \\ \mathbf{B}^*y_r(t) \end{bmatrix}. \qquad (6)$$

Following the servocompensator theory, we next design $u(t)$ to stabilize the system. We will set w, $y_r = 0$ in the design of the stabilizing controller. Since the dynamics of piezo-actuated systems have been known to vary greatly with environmental and load conditions [1], it is desirable for the control to be robustly stabilizing over a range of plant perturbations. We consider a norm-bounded uncertainty [43], where the uncertainty in the plant (1) can be represented by

$$\dot{x}(t) = [A + B_1^* \Delta^* C_1^*]x(t) + [B + B_1^* \Delta^* D_1^*]u(t) \qquad (7)$$

for appropriately defined matrices B_1^*, C_1^*, D_1^*. The matrices B_1^*, C_1^*, D_1^* are known, and represent knowledge of the range of the uncertainties in the matrix/transfer function parameters. The matrix Δ^* is unknown and satisfies the bounds

$$\Delta^* \leq I, \ \Delta^{*'} \Delta^* \leq I$$

where $'$ denotes the transpose, and I is an identity matrix. With this uncertainty, the system (6) becomes

$$\begin{bmatrix} \dot{x}(t) \\ \dot{\eta}(t) \end{bmatrix} = \begin{bmatrix} A + B_1^* \Delta^* C_1^* & 0 \\ -\mathbf{B}^*C & \mathbf{C}^* \end{bmatrix} \begin{bmatrix} x(t) \\ \eta(t) \end{bmatrix} \qquad (8)$$
$$+ \begin{bmatrix} (B + B_1^* \Delta^* D_1^*)u(t) \\ 0 \end{bmatrix}.$$

Define a cost functional

$$J = \int_0^\infty [\gamma' Q\gamma + Ru^2]dt$$
$$\gamma = [x', \eta']', \ Q = Q' \geq 0, \quad R > 0. \qquad (9)$$

We define new matrices

$$\bar{A} = \begin{bmatrix} A & 0 \\ -\mathbf{B}^*C & \mathbf{C}^* \end{bmatrix}, \quad \bar{B} = \begin{bmatrix} B \\ 0 \end{bmatrix}, \quad B_1 = \begin{bmatrix} B_1^* & 0 \\ 0 & 0 \end{bmatrix}$$
$$C_1 = \begin{bmatrix} C_1^* & 0 \\ 0 & 0 \end{bmatrix}, \quad D_1 = \begin{bmatrix} D_1^* \\ 0 \end{bmatrix}$$

where each 0 represents an appropriately defined zero matrix. The following lemma is adapted from [43, Th. 1].

Lemma 1: If for some $\varepsilon = \varepsilon_1^* > 0$, $R = R^* > 0$, there exists a unique positive definite solution $P = P^*$ to the Riccati equation

$$[\bar{A} - \bar{B}(\varepsilon R + D_1' D_1)^{-1} D_1' C_1]' P$$
$$+ P[\bar{A} - \bar{B}(\varepsilon R + D_1' D_1)^{-1} D_1' C_1]$$
$$+ \varepsilon P B_1 B_1' P - \varepsilon P \bar{B}(\varepsilon R + D_1' D_1)^{-1} \bar{B}' P$$
$$+ 1/\varepsilon C_1'(I - D_1(\varepsilon R + D_1' D_1)^{-1} D_1')C_1 + Q = 0 \qquad (10)$$

then for any fixed $\varepsilon \in (0, \varepsilon_1^*)$ and any fixed $R \in (0, R^*)$, (10) has a unique positive definite stabilizing solution P, and the control law $u(t) = -[K_1, K_2]\gamma(t)$ defined via

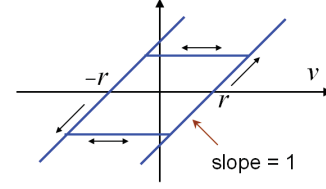$$u(t) = -(\varepsilon R + D_1' D_1)^{-1}(\varepsilon B_1' P + D_1' C_1)\gamma(t) \qquad (11)$$

Fig. 3.   Illustration of a play operator.

guarantees exponential stability of the closed-loop system (8), when $y_r = 0$.

It should be noted that there are many other ways of designing the stabilizing control u. As illustrated in Fig. 1(b), the stabilizing controller $D(s)$ is, in general, a dynamic controller that can be designed using a variety of techniques, such as LQG control and H_∞ control. In addition, while state feedback is used in (11), one can realize output feedback by adopting a state observer, as will be discussed in Section IV-B.

III. ANALYSIS OF THE CLOSED-LOOP SYSTEM

Having designed the stabilizing control $u(t)$ in the absence of hysteresis, we are now prepared to handle the case with hysteresis. In this section, we analyze the tracking performance of the proposed composite controller that combines a servo-compensator with an approximate hysteresis inverse. We first introduce the hysteresis model and its inversion focused in this paper, and then establish the asymptotic stability of the closed-loop system for the tracking error analysis.

A. Hysteresis Modeling and Inversion

In this section, we will focus on the (classical) PI operator for modeling the plant hysteresis. The PI operator consists of a weighted superposition of basic hysteretic units called play operators, shown in Fig. 3. Each play operator P_r is parameterized by a parameter r, which represents the play radius or threshold. The output $u_r(t)$ of a play operator P_r for a continuous, monotone input $v(t)$ over $t \in [0, T]$, is given by

$$u_r(t) = P_r[v; u_r(0)](t) = \max\{\min\{v(t)+r, u_r(0)\}, v(t)-r\}. \qquad (12)$$

The output $u_r(t)$ also represents the current state of the operator P_r. For general inputs, the input signal is broken into monotone segments. The output is then calculated from the successive segments, where the last output of one monotone segment becomes the initial condition for the next. In general, the PI operator is an infinite-dimensional operator, made up of a continuum of play operators integrated over the play radii. In the interest of practical implementation, we consider only a finite-dimensional PI operator where the operator can be represented as a weighted sum of a finite number of play operators. In Section VI, we will briefly discuss the justification of approximating the hysteresis in a real plant like a piezo-actuated system with a finite-dimensional PI operator, and point out a potential approach for analyzing the effect of modeling errors introduced by such approximations.

Assumption 3: The hysteresis nonlinearity is represented by a PI operator Γ_h containing $m + 1$ play operators, where the

radius parameters are assumed to be known and satisfy $0 = r_0 < r_1 < \cdots < r_m < \infty$.

The output of Γ_h under an input v is then given by

$$u(t) = \Gamma_h[v; W(0)](t) = \sum_{i=0}^{m} \theta_i P_{r_i}[v; W_i(0)](t) \qquad (13)$$

where $W_i(t)$ represents the state of the play operator P_{r_i} at time t, and

$$W(t) \triangleq (W_0(t), W_1(t), \ldots, W_m(t))'$$

and $W(0)$ represents the initial condition of the operator Γ_h. The vector $\theta = (\theta_0, \theta_1, \ldots, \theta_m)' \geq 0$ represents the weights of individual play elements of the operator and is assumed to be finite. We will use $\mathbf{r}$ to denote the vector of radii, $\mathbf{r} = (r_0, r_1, \ldots, r_m)'$. We also define the operator $\mathcal{P} \triangleq (P_{r_0}, P_{r_1}, \ldots, P_{r_m})'$, which captures the evolution of the state $W(t)$ of Γ_h under input v

$$W(t) = \mathcal{P}[v; W(0)](t). \qquad (14)$$

The inverse Γ_h^{-1} of a finite-dimensional PI operator Γ_h can be analytically constructed, which turns out to be another PI operator. The radii, weights, and initial conditions of the play operators realizing Γ_h^{-1} can be calculated explicitly in terms of those for Γ_h, see [25, Eqs. (12)–(14)].

To accommodate uncertainties in our knowledge about the actual hysteresis model Γ_h, we assume that we do not know the exact value of the weight vector θ; instead, we only have an estimate, denoted as $\hat{\theta}$, for θ. On the other hand, as mentioned in Assumption 3, we assume that the exact values of the play radii $\mathbf{r}$ are known. The latter is a common assumption when modeling hysteresis with the PI operator [25], [30], [42]. Through proper initialization, for example, by sweeping the input from $-r_m$ to r_m, we can set the initial state $W(0)$ for Γ_h. We use $\hat{\Gamma}_h$ to denote the PI operator with radii $\mathbf{r}$ and weights $\hat{\theta}$. Recall again Fig. 1. Given an initial condition $W(0)$ and a desired trajectory u_d for the forward hysteresis model Γ_h, its input v is generated by inverting the approximate hysteresis model $\hat{\Gamma}_h$

$$v(t) = \hat{\Gamma}_h^{-1}[u_d; W(0)](t) = \sum_{i=0}^{m} \vartheta_i P_{\varphi_i}[u_d; Z_i(0)](t). \qquad (15)$$

Here the operator $\hat{\Gamma}_h^{-1}$ represents the inverse of $\hat{\Gamma}_h$. In implementation, $\hat{\Gamma}_h^{-1}$ is realized as another PI operator taking u_d as input, and the radii φ_i, weights ϑ_i, and initial conditions $Z_i(0)$, $i = 0, \ldots, m$, of the play elements for the latter PI operator are computed based on $\mathbf{r}$, $\hat{\theta}$, and $W(0)$ following the formula in [25]. With (15), we can rewrite $u_d(t)$ as

$$u_d(t) = \hat{\Gamma}_h[v; W(0)](t) = \sum_{i=0}^{m} \hat{\theta}_i P_{r_i}[v; W_i(0)](t). \qquad (16)$$

Subtracting (13) from (16), we obtain

$$u_d(t) - u(t) = \tilde{\theta}' W(t) \qquad (17)$$

where $\tilde{\theta} \triangleq \hat{\theta} - \theta$.

B. Asymptotic Stability of the Closed-Loop System

Recall Fig. 1. Note that the controller is a composite of a servocompensator/stabilizing controller and an approximate inverse compensator of hysteresis. We will assume that the exosystem (2) contains a finite number of harmonics of the reference trajectory. To apply the linear servocompensator theory as outlined in Section II, however, we need to establish that the inversion error $u_d - u$, which is in the loop, can indeed be treated equivalently as an exogenous periodic disturbance.

We assume that the uncertainty in the plant takes the form of (7). We define $\mathcal{B} \triangleq (B + B_1^* \Delta^* D_1^*)$ for ease of notation. We let u_d act as our desired stabilizing input (11). Under state feedback (11) (with u replaced by u_d), we have

$$u_d(t) = -[K_1, K_2]\gamma(t). \qquad (18)$$

With (8) and (17) (for a non-zero reference y_r) becomes

$$\dot{\gamma}(t) = \begin{bmatrix} A + B_1^* \Delta^* C_1^* - \mathcal{B}K_1 & -\mathcal{B}K_2 \\ -\mathbf{B}^* C & \mathbf{C}^* \end{bmatrix} \gamma(t) + \begin{bmatrix} \mathcal{B}(-\tilde{\theta}' W(t)) \\ \mathbf{B}^* y_r(t) \end{bmatrix}. \qquad (19)$$

Note that the vector $W(t)$ is governed by the following hysteresis operators:

$$W(t) = \mathcal{W}[u_d; W(0)](t) \triangleq \mathcal{P} \circ \hat{\Gamma}_h^{-1}[u_d; W(0)](t) \qquad (20)$$

where "$\circ$" denotes the composition of operators.

Equations (18)–(20), form a complete description of the closed-loop system, which clearly shows the coupling of an ODE with a hysteresis operator. The system can be analyzed with a perturbation technique introduced in [47], where the nominal (non-hysteretic) system is obtained by letting $\tilde{\theta} = 0$ in (19). From the linear systems theory, for a T−periodic reference trajectory y_r, the solution $\gamma(t)$ of the nominal system converges exponentially to a (unique) periodic function γ_T.

Define $u_{dT} = -[K_1, K_2]\gamma_T$ and $v_T = \hat{\Gamma}_h^{-1}[u_{dT}; W(0)]$. Note that u_{dT} is T−periodic, and v_T is also T−periodic (after a duration of T seconds, to be precise). For any continuous function f, define the oscillation function osc by

$$\mathrm{osc}_{[t_1, t_2]}[f] = \sup_{t_1 \leq \tau \leq \sigma \leq t_2} |f(\tau) - f(\sigma)|. \qquad (21)$$

In order to show the asymptotic stability of a periodic solution, we will require that the hysteresis operator $\mathcal{W}$ obey a contraction property. This can be guaranteed with the following assumptions.

Assumption 4: $\mathrm{osc}_{[0,T]}[u_{dT}] > 2\varphi_m$, and $\mathrm{osc}_{[T,2T]}[v_T] > 2r_m$, where we recall that φ_m and r_m are the largest play radii for the PI operators $\hat{\Gamma}_h^{-1}$ and Γ_h, respectively.

Theorem 1: Let the reference trajectory y_r be T−periodic. Let Assumptions 1–4 hold. Then there exists $\varepsilon_2^* > 0$, such that, if the Euclidean norm of $\tilde{\theta}$, denoted as $\|\tilde{\theta}\|$, satisfies $\|\tilde{\theta}\| \leq \varepsilon_2^*$, then the solution of the closed-loop system (18), (19), and (20) under any initial condition $(\gamma(0), W(0))$ will converge asymptotically to a unique periodic solution.

Proof: Assumption 4 implies that the composite hysteretic operator $\mathcal{W}$ has a contraction property, in particular, for two different initial conditions $W_a(0)$ and $W_b(0)$

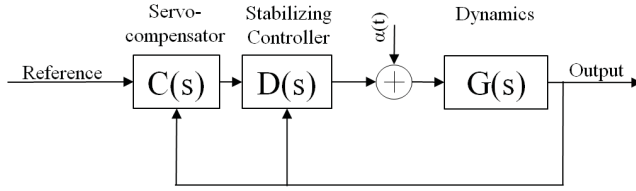$$|\mathcal{W}[u_d; W_a(0)](t) - \mathcal{W}[u_d; W_b(0)](t)| = 0 \qquad (22)$$

Fig. 4.　Equivalent system block diagram for steady-state analysis.

for $t \geq 2T$, as shown in [32]. Indeed, for a play operator with radius r, its state will be independent of the initial condition once its input varies (over time) by at least $2r$. This can be proven through elementary analysis on the play operator. The operator $\mathcal{W}$ is a composition of $\mathcal{P}$ (a stack of play operators with the largest radius being r_m) and $\hat{\Gamma}^{-1}$ (a superposition of play operators with the largest radius being φ_m), therefore the contraction property in (22) is easily established.

Write $\tilde{\theta} = \varepsilon \tilde{\theta}_0$, where $\tilde{\theta}_0$ is a unit vector in the direction of $\tilde{\theta}$. We also note that the PI operator satisfies a Lipschitz condition [32], as well as the Volterra and semi-group properties [9]. Finally, we know from the definition of the PI operator that there exist constants a_g and b_g such that the growth condition

$$\|W(t)\| \leq a_g |u_d(t)| + b_g \quad \forall t \tag{23}$$

is satisfied, which, together with (18), implies

$$\|W(t)\| \leq \bar{a}_g \|\gamma(t)\| + \bar{b}_g \tag{24}$$

for some constants $\bar{a}_g, \bar{b}_g > 0$. Since the nominal system with $\tilde{\theta} = 0$ is globally T−convergent about γ_T [47], (18)–(20) fits into the class of systems considered [47, Th. 2.1]. This establishes the existence of a unique, asymptotically stable periodic solution when ε, or equivalently, $\tilde{\theta}$, is sufficiently small. ∎

C. Tracking Error Analysis

From Theorem 1, given the composite controller (servo-compensator and inverse hysteresis compensator), the closed-loop signals, including the inversion error $\tilde{\theta}' W(t)$, converge to T−periodic signals that depend only on the reference signal y_r. Therefore, in analysis, one can essentially treat the inversion error at the steady state as a matched, exogenous disturbance, as illustrated in Fig. 4. We can now make use of the periodicity of $W(t)$ in the tracking error analysis. From the T−periodicity of $W(t)$, we can write

$$\alpha(t) = \tilde{\theta}' W(t) = c_0 + \sum_{k=1}^{\infty} c_k \sin\left(\frac{2\pi kt}{T} + \phi_k\right) \tag{25}$$

which can be broken into compensated and uncompensated parts. Define $\mathcal{A}_c$ as the set of all k's such that the internal model of $\sin(2\pi kt/T)$ is accommodated in $\mathbf{C}^*$, and then define

$$\alpha_c = c_0 + \sum_{k \in \mathcal{A}_c} c_k \sin\left(\frac{2\pi kt}{T} + \phi_k\right)$$

$$\alpha_d = \sum_{n \notin \mathcal{A}_c} c_k \sin\left(\frac{2\pi kt}{T} + \phi_k\right). \tag{26}$$

Remark 2: It is assumed in the definition of α_c that an offset term is included in the reference trajectory $y_r(t)$, which is typical in practical applications.

Since we have established that the hysteresis inversion error at the steady state is effectively an exogenous disturbance to an exponentially stable linear system, we can use the superposition principle to analyze the steady state tracking error. We will treat y_r, α_c, and α_d as three different inputs to the system. Write

$$e(t) = y_r(t) - Cx = y_r(t) - (y_1(t) + y_2(t) + y_3(t)) \tag{27}$$

where y_i, $i = 1, \ldots, 3$, will be defined shortly. First, consider the signal $y_1(t)$, which arises when α_c, $\alpha_d = 0$. By Theorem 1 of [45] and Lemma 1, this part of the response will approach y_r as $t \to \infty$. Next, we consider the output response when y_r, $\alpha_d = 0$, which we will define as $y_2(t)$. Since α_c is comprised entirely of signals whose internal models are contained in $\mathbf{C}^*$, [45, Th. 1] states that the response of this system will asymptotically track the reference trajectory, which in this case is zero. Finally, we consider the output when y_r, $\alpha_c = 0$, which is denoted as $y_3(t)$. In this case, α_d will not be accommodated in the servocompensator design. Since the closed-loop system is a stable linear system and α_d is bounded, the output response from this portion is bounded and on the order of α_d. From these discussions, the tracking error under the proposed control scheme will be of the order of α_d, which can be made arbitrarily small by accommodating a sufficient number of harmonics in the servocompensator design.

IV. EXTENSIONS OF THEOREM 1

In this section, we present two extensions to Theorem 1, which will allow the proposed method to be applied to more general systems. In the first extension, we consider a modified PI operator, which is more versatile than the classical PI operator in capturing physical hysteresis phenomena. The second extension deals with using output feedback in the stabilizing controller.

A. Extension to the Case Involving a Modified PI Operator

A shortfall of the classical PI operator is that it cannot capture asymmetric hysteresis, due to the odd symmetry of play operators. In [25], a weighted superposition of (memory-free) one-sided dead-zone operators is proposed to be combined with a classical PI operator to create a *modified* PI operator, capable of modeling non-symmetric hysteresis phenomena. For a one-sided dead-zone operator d_{z_i} with input $v(t)$ and threshold z_i, its output obeys the equation

$$d_{z_i}(v(t)) = \begin{cases} \max(v(t) - z_i, 0), & z_i > 0 \\ v(t), & z_i = 0 \\ \min(v(t) - z_i, 0), & z_i < 0. \end{cases} \tag{28}$$

Now denote the vector $z = [z_{-l}, \ldots, z_{-1}, z_0, z_1, \ldots, z_l]'$, where

$$-\infty < z_{-l} < \cdots < z_{-1} < z_0 = 0 < z_1 < \cdots < z_l < \infty$$

and consider a vector of weights $\theta_d = [\theta_{d-l}, \ldots, \theta_{d-1}, \theta_{d0}, \theta_{d1}, \ldots, \theta_{dl}]'$ that is nonnegative and
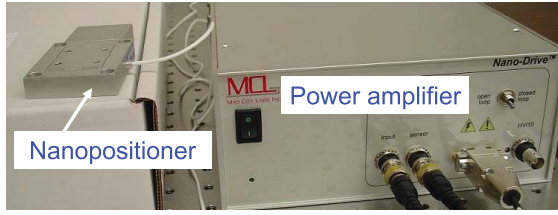
Fig. 5. Nanopositioning stage used in experimentation, Nano-OP65 nanopositioning stage coupled with a nano-drive controller from Mad City Labs Inc. Position feedback is provided by a built-in capacitive sensor.

Fig. 6. Measured hysteresis loops for the nanopositioner.

finite. We define a vector of dead-zone operators $D_z(v(t))$ with thresholds z and input $v(t)$ as

$$D_z(v(t)) = [d_{z_{-l}}(v(t)), \ldots, d_{z_{-1}}(v(t)), d_{z_0}(v(t)),$$
$$d_{z_1}(v(t)), \ldots, d_{z_l}(v(t))]'.$$

The modified PI operator is then defined as a composition of the weighted superposition of operators D_z and a PI operator Γ_h, in particular, the output $u(t)$ of a modified PI operator under an input v and with the initial condition $W(0)$ for Γ_h can be written as

$$u(t) = \Gamma_{\text{hd}}[v; W(0)](t) \triangleq \sum_{j=-l}^{l} \theta_{d_j} d_{z_j} \left(\sum_{i=0}^{m} \theta_i P_{r_i}[v; W_i(0)](t) \right)$$
$$= \theta_d' D_z(\theta' W(t)) \triangleq \Gamma_{\text{hd}}[v, W(0)](t) \quad (29)$$

where we recall θ denotes the weights of the play operators for Γ_h. As with the PI operator, the modified PI operator possesses a closed-form inversion, see [25, Eqs. (23), (25), and (27)]. Similar to the case of a classical PI operator, we make the following assumption.

Assumption 5: It is assumed that the play radii **r** and the dead-zone thresholds z for the modified PI operator are known.

The weights θ for the play operators, and θ_d for the deadzone operators are not known, but we have their estimates, denoted as $\hat{\theta}$ and $\hat{\theta}_d$, respectively. We will denote the modified PI operator with weight vectors $\hat{\theta}$ and $\hat{\theta}_d$ as $\hat{\Gamma}_{\text{hd}}$. Given an initial condition $W(0)$ and a desired trajectory u_d for the forward hysteresis model Γ_{hd}, its input v is generated by inverting the approximate hysteresis model $\hat{\Gamma}_{\text{hd}}$

$$v(t) = \hat{\Gamma}_{\text{hd}}^{-1}[u_d; Z(0)](t) \triangleq \sum_{i=0}^{m} \vartheta_i P_{\varphi_i} \left[\sum_{j=-l}^{l} \xi_i d_{\zeta_i}(u_d); Z_i(0) \right](t) \quad (30)$$

Here, the operator $\hat{\Gamma}_{\text{hd}}^{-1}$ represents the inverse of $\hat{\Gamma}_{\text{hd}}$. In implementation, $\hat{\Gamma}_{\text{hd}}^{-1}$ is realized as a composition of a new PI operator and the weighted superposition of $(2l + 1)$ new dead-zone operators taking u_d as input. The radii φ_i, weights ϑ_i, and initial conditions $Z_i(0)$, $i = 0, \ldots, m$, of the play elements for the latter PI operator are computed based on **r**, $\hat{\theta}$, and $W(0)$, while the thresholds ζ_i and weights ξ_i, $i = -l, \ldots, l$, of the latter dead-zone operators are computed based on z and $\hat{\theta}_d$ [25]. Note that the order of the play operators and dead-zones is reversed in the inverse operator. Following (30), we have

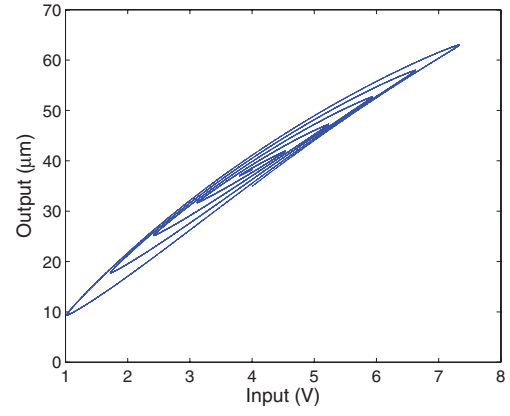$$u_d(t) = \hat{\Gamma}_{\text{hd}}[v; W(0)](t) = \hat{\theta}_d' D_z(\hat{\theta}' W(t)). \quad (31)$$

Having presented the fundamentals about the modified PI operator and its inverse, we are now prepared to discuss the extension of Theorem 1 to a system with such an operator. In order to utilize the framework presented in [47] to show that the system possesses an asymptotically stable periodic solution, we need to show that, under proper assumptions, the hysteretic perturbation (i.e., the inversion error $u_d - u$) to the nominal system can be made arbitrarily small. Subtracting (31) from (29), we have

$$u_d - u = \hat{\theta}_d' D_z(\hat{\theta}' W(t)) - \theta_d' D_z(\theta' W(t))$$
$$= \hat{\theta}_d' D_z(\hat{\theta}' W(t)) - \theta_d' D_z(\theta' W(t)) + \hat{\theta}_d' D_z(\theta' W(t))$$
$$- \hat{\theta}_d' D_z(\theta' W(t)) \quad (32)$$
$$= (\hat{\theta}_d' - \theta_d') D_z(\theta' W(t)) + \hat{\theta}_d' [D_z(\hat{\theta}' W(t))$$
$$- D_z(\theta' W(t))]. \quad (33)$$

It can be easily seen that the dead-zone operator obeys the Lipschitz condition

$$|d_{z_i}(a) - d_{z_i}(b)| \leq |a - b| \quad (34)$$

for any threshold z_i. Using this property, we derive from (33)

$$|u_d - u| \leq \|\tilde{\theta}_d\| \|D_z(\theta' W(t))\| + \|\hat{\theta}_d\|_\infty [(2l + 1)|\tilde{\theta}' W(t)|]$$
$$\leq \|\tilde{\theta}_d\| \|D_z(\theta' W(t))\| + \|\hat{\theta}_d\|_\infty [(2l + 1)\|\tilde{\theta}\| \|W(t)\|]$$
$$\leq \varepsilon(\|D_z(\theta' W(t))\| + (2l + 1)\|\hat{\theta}_d\|_\infty \|W(t)\|) \quad (35)$$

where $\varepsilon = \max(\|\tilde{\theta}\|, \|\tilde{\theta}_d\|)$, and $\| \cdot \|$ and $\| \cdot \|_\infty$ denote the Euclidean norm and the infinity-norm of a vector, respectively. From (35), we see that the amount of the hysteretic perturbation to the nominal system is directly dependent on parameter errors $\tilde{\theta}$ and $\tilde{\theta}_d$, and can be made arbitrarily small when the weight parameters are sufficiently accurate.

Finally, we must show that the modified PI operator obeys a contraction property similar to that in (22). Since the added dead-zone operators do not have memory (or states), the contraction property holds for them automatically. Therefore, the contraction property for the composite hysteresis operator rests on that for the play elements in both the modified PI operator and its inverse, the condition of which can be formulated similarly as in Assumption 4. The primary difference is that the input to the play elements in the inverse operator
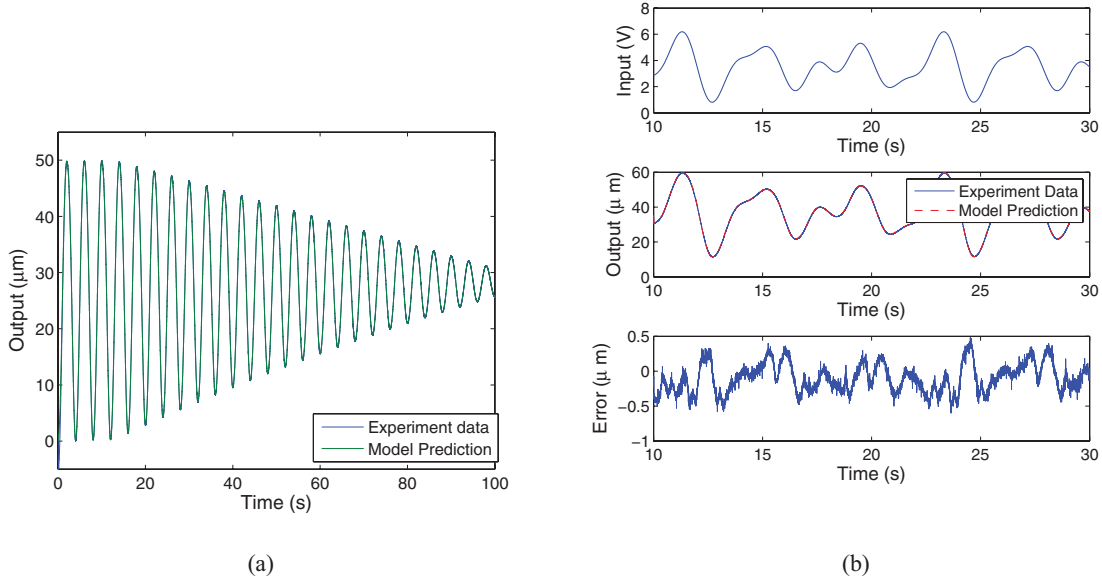
(a)   (b)

Fig. 7. (a) Plant output used in the identification of the modified PI operator and the resulting model output, under a quasi-static, oscillatory input with decreasing amplitude. (b) Validation of the identified hysteresis model using a quasi-static input different from that used in the model identification.
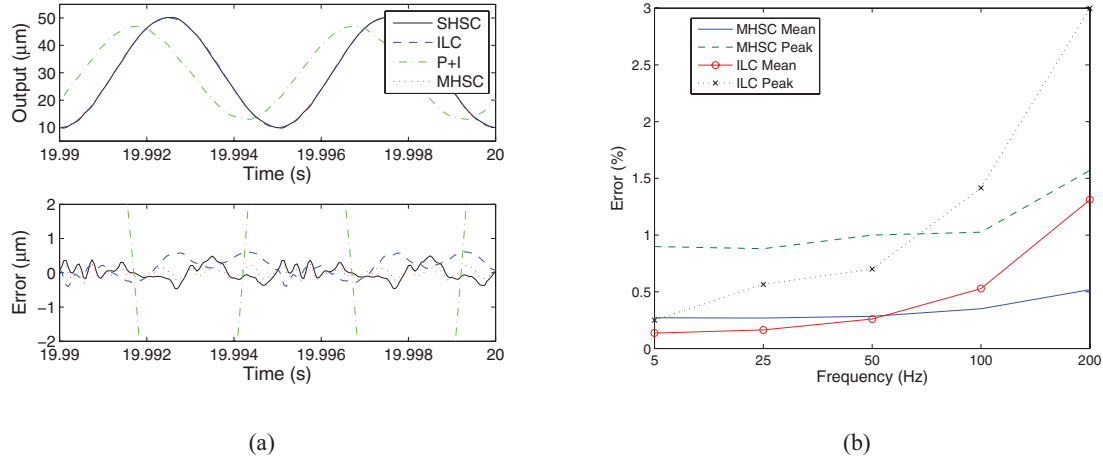

(a)   (b)

Fig. 8. (a) Experimental results at 200 Hz for the proposed methods (SHSC and MHSC), ILC and P+I. (b) Comparison between MHSC and ILC.

is now $\sum_{i=-l}^{l} \xi_i d_{\zeta_i}(u_d)$ instead of u_d. Based on the above discussions, we can formally state the following theorems.

Theorem 2: Consider Fig. 1, where the hysteresis is modeled with a modified PI operator. Let the reference trajectory y_r be T−periodic, and let Assumptions 1, 2, and 5 hold. The closed-loop system is described by

$$\dot{\gamma}(t) = \begin{bmatrix} A + B_1^* \Delta^* C_1^* - \mathcal{B} K_1 & -\mathcal{B} K_2 \\ -\mathbf{B}^* C & \mathbf{C}^* \end{bmatrix} \gamma(t)$$
$$+ \begin{bmatrix} -\mathcal{B}[\hat{\theta}_d' D_z(\hat{\theta}' W(t)) - \theta_d' D_z(\theta' W(t))] \\ \mathbf{B}^* y_r(t) \end{bmatrix} \quad (36)$$

$$W(t) = \bar{\mathcal{W}}[u_d; W(0)](t) \triangleq \mathcal{P} \circ \hat{\Gamma}_{\text{hd}}^{-1}[u_d; W(0)](t) \quad (37)$$

$$u_d(t) = -[K_1, K_2]\gamma(t) \quad (38)$$

With suitably chosen gain matrices K_1 and K_2, when $\tilde{\theta} = 0$, $\tilde{\theta}_d = 0$, the solution $\gamma(t)$ converges exponentially to a unique periodic function γ_T. Furthermore, define $u_{dT} =$

$-[K_1, K_2]\gamma_T$, and $v_{dT} = \hat{\Gamma}_{\text{hd}}^{-1}[u_{dT}; W(0)]$. Assume

$$\text{osc}_{[0,T]} \left[\sum_{i=-l}^{l} \xi_i d_{\zeta_i}(u_d) \right] > 2\varphi_m \quad (39)$$

$$\text{osc}_{[T,2T]}[v_T] > 2r_m. \quad (40)$$

Then there exists $\varepsilon_3^* > 0$, such that, if $\max(\|\tilde{\theta}\|, \|\tilde{\theta}_d\|) \leq \varepsilon_3^*$, the solution of (36)–(38) under any initial condition $(\gamma(0), W(0))$ will converge asymptotically to a unique periodic function.

With Theorem 2, tracking error analysis can be conducted similarly as in Section III-C.

B. Extension to the Case of Output Feedback

In (18) and (38), state feedback is used for the stabilizing controller. When the state x is not accessible, output feedback

TABLE I

TRACKING ERROR RESULTS FOR VARIOUS CONTROLLERS. ALL RESULTS ARE PRESENTED AS A PERCENTAGE OF THE
REFERENCE AMPLITUDE (20 μm)

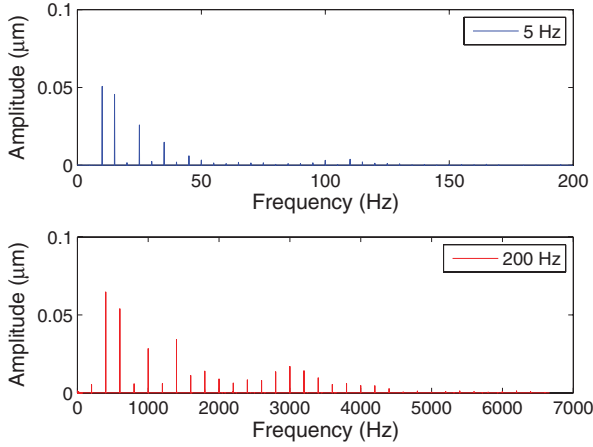| Reference	MHSC (%)		SHSC (%)		ILC (%)		P+I (%)	
	avg($|e(t)|$)	max($|e(t)|$)	avg($|e(t)|$)	max($|e(t)|$)	avg($|e(t)|$)	max($|e(t)|$)	avg($|e(t)|$)	max($|e(t)|$)
Sine, 5 Hz	0.271	0.899	0.649	1.72	0.135	0.250	1.06	1.93
Sine, 25 Hz	0.268	0.881	0.707	1.85	0.163	0.565	5.40	8.96
Sine, 50 Hz	0.284	1.01	0.770	1.93	0.262	0.711	10.86	17.63
Sine, 100 Hz	0.352	1.03	0.815	2.38	0.528	1.42	21.21	33.65
Sine, 200 Hz	0.519	1.57	0.863	2.50	1.31	3.20	37.61	59.6

Fig. 9. Frequency spectra of the tracking error signal for references at 5 and 200 Hz. An SHSC was used in each case. Graphs are aligned so that the peaks on each graph correspond to the same harmonic of the reference. Note the prominence of the harmonics near 3000 Hz in the 200-Hz plot.

Fig. 10. Experimental results at 50 Hz for sawtooth reference signal. Two periods are shown.

will be required. One such approach is to estimate the state with an observer and then plug the estimate into the state feedback control law. Here we perform the analysis of the closed-loop system when a Luenberger observer is used for state estimation, which is what we adopted in experimental implementation of the proposed control approach. For this analysis, we will assume no uncertainty in the linear dynamics (i.e., $\Delta^* = 0$) and consider the modified PI operator. The observer equation and the output feedback control law are as follows:

$$\dot{\hat{x}}(t) = A\hat{x}(t) + Bu_d(t) + L(y(t) - C\hat{x}(t)) \quad (41)$$

$$u_d(t) = -[K_1, K_2]\begin{bmatrix} \hat{x}(t) \\ \eta(t) \end{bmatrix}. \quad (42)$$

The closed-loop system is then, for $\gamma = [x', \eta', \hat{x}']'$

$$\dot{\gamma}(t) = \begin{bmatrix} A & -BK_2 & -BK_1 \\ -\mathbf{B}^*C & \mathbf{C}^* & 0 \\ LC & -BK_2 & A - BK_1 - LC \end{bmatrix} \gamma(t)$$
$$+ \begin{bmatrix} -B[\hat{\theta}'_d D_z(\hat{\theta}' W(t)) - \theta'_d D_z(\theta' W(t))] \\ \mathbf{B}^* y_r(t) \\ 0 \end{bmatrix} \quad (43)$$
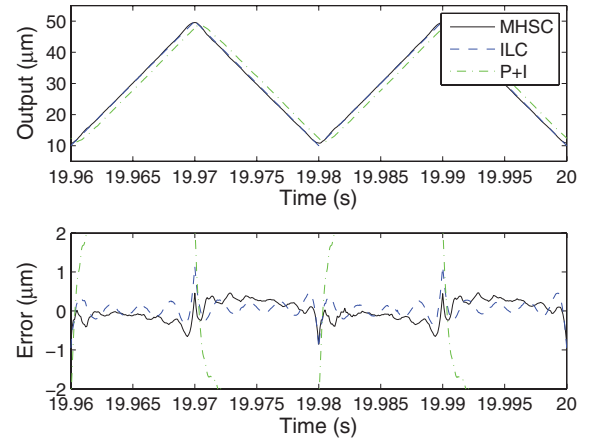
where $W(t)$ evolves according to (37). When $\tilde{\theta} = 0$, $\tilde{\theta}_d = 0$, we obtain the nominal system from (43) that has no hysteretic perturbation. We can choose the observer gain vector L, so that the resulting nominal system is exponentially stable when $y_r \equiv 0$, and admits a unique exponentially stable T−periodic solution for T−periodic y_r. From here on, the analysis will follow the developments in Theorem 2, and we can conclude that, with proper "oscillation conditions" for u_{dT} and v_T [similar to (39) and (40)], for sufficiently small $\tilde{\theta}$ and $\tilde{\theta}_d$, the closed-loop system with output feedback, (37), (41)–(43) will have a unique, asymptotically stable periodic solution. Note that the estimation error $\tilde{x} \triangleq \hat{x} - x$ will obey the differential equation

$$\dot{\tilde{x}}(t) = (A - LC)\tilde{x}(t) - B[\hat{\theta}'_d D_z(\hat{\theta}' W(t)) - \theta'_d D_z(\theta' W(t))]$$

which implies that $\tilde{x}$ will be at the order of $u_d - u$ and not vanish at the steady state. On the other hand, since all signals at the steady state are T−periodic, we can follow the same argument as in Section III-C for the tracking error analysis, and conclude that the tracking error can be made arbitrarily small when the servocompensator accommodates the internal models of a sufficient number of harmonic components.

While the above analysis on the output feedback case assumes perfectly known linear dynamics, our experimental
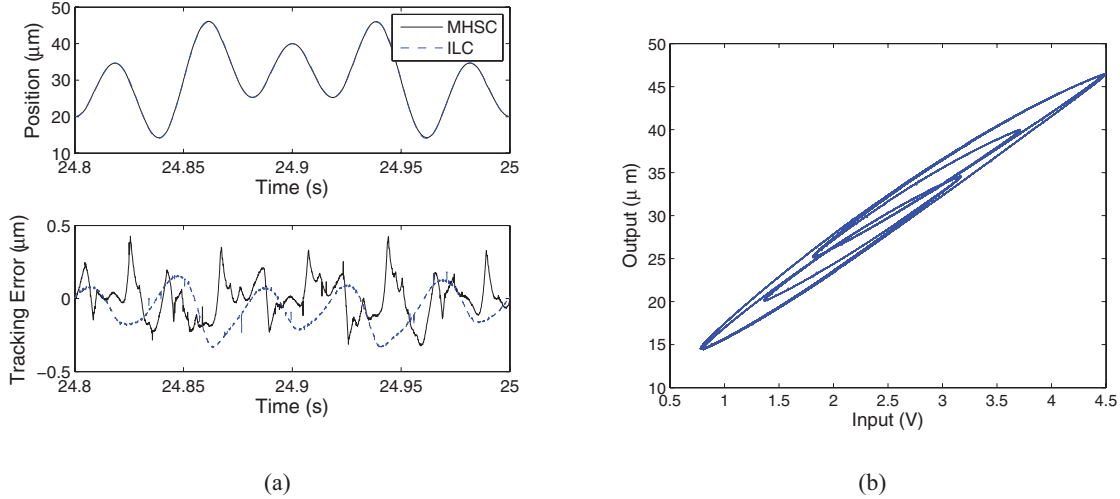
Fig. 11.   (a) Experimental results for a reference trajectory of $y_r = 5\sin(2\pi 5t - \pi/2) + 5\sin(2\pi 15t + \pi/2) + 10\sin(2\pi 25t - \pi/2)$. (b) Hysteresis loops of nanopositioning stage in tracking a reference trajectory of $y_r = 5\sin(2\pi 5t - \pi/2) + 5\sin(2\pi 15t + \pi/2) + 10\sin(2\pi 25t - \pi/2)$.

results (to be presented in the next section) indicate that the proposed method enjoys robustness to changes in the system dynamics.

V. EXPERIMENTAL RESULTS

A. Setup and Modeling

Experiments were conducted on a piezo-actuated nanopositioner (Fig. 5) to examine the performance of the proposed control scheme. The first step of these experiments is to identify the model of the piezo-actuated system as shown in Fig. 1(b). The hysteretic behavior was experimentally characterized with a quasi-static input. As shown in Fig. 6, the hysteresis loop is not odd-symmetric. Following [25], we used a modified PI operator, consisting of a superposition operator with nine dead-zone elements in conjunction with a PI operator with eight play elements to model the asymmetric hysteresis. This model was identified *offline* using the quadratic optimization routine outlined in [25], The radii **r** and thresholds z were chosen based on the input and output ranges of the plant

$$\mathbf{r} = [0, 0.33, 0.66, 1.00, 1.33, 1.66, 2.00, 2.33]'$$
$$z = [-2.68, -1.97, -1.22, -0.42, 0, 0.32, 1.02, 1.76, 2.57]'$$

and the resulting model weights were

$$\hat{\theta} = [0.719, 0.183, 0.035, 0.055, 0.034, 0.033, 0.023, 0.061]'$$
$$\hat{\theta}_d = [1.062, 0.473, 0.641, 0.311, 8.426, -0.636, -0.501,$$
$$\quad -0.614, -0.415]'$$

which were used to calculate the output of the inverse operator, $\hat{\Gamma}_{hd}^{-1}[u_d; W(0)](t)$. Fig. 7(a) shows the system output under a quasi-static, oscillatory input with decreasing amplitude, and the input/output data were used for identification of the weights. Also shown in the figure was the output prediction by the resulting model, with largest discrepancy with the measurement being around 1 μm. To further validate the model, a different quasi-static input comprising a summation of sinusoids was applied to the piezo-actuated nanopositioner.

Within each period, the input has multiple distinct maxima and minima, and is thus expected to excite multiple memory states of the hysteresis. Fig. 7(b) shows the model output and the measured output, where we can see that the modeling error is around 1 μm for a travel range of 45 μm. The comparisons in Fig. 7(a) and (b) indicate that, while the identified model was not perfect, it provided a good approximation to the hysteresis behavior of the nanopositioner.

The plant dynamics was identified based on the frequency response obtained with small-amplitude sinusoidal inputs. The MATLAB function *invfreqs* was used to identify the linear dynamics model. In the absence of any load, we found that a fourth-order plant model matched the measured frequency response reasonably well, up to 3.5 kHz. This model has the transfer function

$$G(s) = \frac{8.8 \times 10^{16}}{s^4 + 1.6 \times 10^4 s^3 + 6.6 \times 10^8 s^2 + 5.3 \times 10^{12} s + 8.8 \times 10^{16}}.$$
(44)

In order to improve the computation accuracy, we used a balanced state-space realization [48, Eq. 44]. This results in the model

$$\dot{x}(t) = 1.0 \times 10^4 \begin{bmatrix} -0.014 & 1.700 & 0.095 & -0.050 \\ -1.700 & -0.241 & -0.672 & 0.170 \\ 0.095 & 0.672 & -1.066 & 1.617 \\ 0.050 & 0.170 & -1.617 & -0.305 \end{bmatrix} x(t)$$

$$+ \begin{bmatrix} 27.8 \\ 111.3 \\ -116.5 \\ -44.1 \end{bmatrix} u(t)$$

$$y(t) = \begin{bmatrix} 27.8 & -111.3 & -116.5 & 44.1 \end{bmatrix} x(t).$$
(45)

We next designed our robust stabilizing control (11). First, we tested how the model parameters varied with loads. Based on this, we found that with a maximum load the first resonant frequency of the plant changes by around 5%, with similar changes in the damping ratio and other resonant frequencies. Therefore, we designed our controller to be robust to changes

TABLE II

TRACKING ERRORS RESULTS FOR SAWTOOTH REFERENCES.
ALL RESULTS ARE PRESENTED AS A PERCENTAGE OF THE
REFERENCE AMPLITUDE (20 μm)

	5 Hz (%)		50 Hz (%)	
	avg($|e(t)|$)	max($|e(t)|$)	avg($|e(t)|$)	max($|e(t)|$)
MHSC	0.562	4.15	1.08	4.26
ILC	0.114	0.775	0.808	5.70
P+I	1.08	1.30	10.3	12.1

TABLE III

LOADING PERFORMANCE FOR MHSC AND ILC. ALL RESULTS ARE
PRESENTED AS A PERCENTAGE OF THE REFERENCE AMPLITUDE (20 μm)

	avg($|e(t)|$)	max($|e(t)|$)	% Change from unloaded	
MHSC	0.288	0.940	1.41	−6
ILC	0.308	0.775	18.5	10.7

of ±10% in the parameters in our state space model. We used this guideline to formulate the matrices B_1, C_1, and D_1 in (7). We then translated this constraint into balanced coordinates via the same coordinate transformation used to generate (45). The resulting matrices become the B_1, C_1, and D_1 matrices used in (10), and along with the balanced coordinate system matrices from (45) were used to calculate the stabilizing control (11).

Finally, we implemented a Luenberger observer to estimate the states, as explored in Section IV-B. Designed and implemented in the standard manner with the nominal state space model of the plant (i.e., $\Delta^* = 0$), the output feedback controller is given as

$$\dot{\hat{x}} = A\hat{x} + Bu_d + L(y - C\hat{x}) \tag{46}$$

$$u_d = -[K_1, K_2]\begin{bmatrix}\hat{x}(t)\\\eta(t)\end{bmatrix} \tag{47}$$

where L is chosen so that $A - LC$ is Hurwitz. In our work, L was chosen using an LQR method, and was $[0.3, -3.5, -1.7, -0.23]$.

B. Results

In the tracking experiments, sinusoids of 5, 25, 50, 100, and 200 Hz were utilized for reference signals, with the travel range of 40 μm and a 30-μm offset. Note that the used frequencies are well within the working frequency range of typical SPM systems. For example, the SPM system described in [49] could produce a single scan line in 5 ms, which translates to a 100-Hz reference signal. Control and measurement in our experiments were facilitated by a dSPACE platform. For comparison, we implemented an ILC algorithm [15]. We also used a custom-designed proportional-integral (P+I) controller followed by hysteresis inversion. Two different types of servocompensators were used in experiments. First, a single-harmonic servocompensator (SHSC) was designed, including the internal model of only the reference signal. Second, we designed a MHSC, including the internal model of the reference signal as well as its second and third harmonics.

Two metrics are used to quantify the tracking error. The mean tracking error is computed by taking the average of $|e(t)|$ over one period of the reference input, and the peak tracking error is the maximum tracking error. Table I contains the results on tracking error for each controller at different frequencies. The P+I controller performs very poorly at high frequencies, a problem that has been well documented [1]. The ILC algorithm performs very well in general, but cannot match the MHSC at 200 Hz, which can also be seen in Fig. 8(a).

A detailed comparison between the two methods is shown in Fig. 8(b). At low frequencies, the ILC algorithm performs better than the MHSC. At 50 Hz, the errors are very close, with ILC still ahead. However, at 100 and 200 Hz, the MHSC is significantly better, with only 40% the mean tracking error of ILC at 200 Hz.

We can also compare the performance of the MHSC with that of the SHSC. From our theory, we would expect the MHSC to perform significantly and consistently better than the SHSC. The results of Table I confirm this expectation, as the MHSC outperforms the SHSC by significant margins at each frequency for both error metrics. However, the differences get closer together as the reference frequency increases. At 5 Hz, the MHSC has around 40% of the tracking error of the SHSC, whereas at 200 Hz the MHSC has 60%. This is due to the effect of the resonant peak of the vibrational dynamics on the harmonics generated by the hysteresis. In particular, with increasing frequencies, the harmonics higher than the second and third become more significant. We can see this clearly by comparing the tracking error frequency spectra under SHSC and MHSC, respectively. Fig. 9 shows the spectra under SHSC for reference signals at 5 and 200 Hz. In both cases, the second and third harmonics of the reference signal are the most significant in the error signal. However, the other harmonics of the system at 200 Hz are significantly larger in comparison to the dominant harmonics than they are at 5 Hz. It is, therefore, reasonable to expect that canceling the second and third harmonics in the 200-Hz case would result in reduced benefit as compared to that in the 5-Hz case.

We also demonstrated the ability for the MHSC to track sawtooth reference signals. Sawtooth signals are commonly used in SPM applications, and represent a challenge for servocompensaton since they do not have a finite-dimensional internal model. However, by using the first few harmonics of the signal, we can arrive at a reasonable approximation. Fig. 10 and Table II shows tracking error results for the three control methods used, where the MHSC incorporated the first six odd harmonics of the reference. The ILC controller is well suited to tracking signals like a sawtooth, and this is shown in the tracking results. While the P+I controller has reasonable performance at 5 Hz, its performance falls off dramatically at 50 Hz. The MHSC does a significantly better job than the P+I controller at tracking this signal, with an average error that was only 20% of what was achieved by the latter controller at 50 Hz. While the tracking error under the MHSC is almost five times of that under ILC, it becomes comparable to that of ILC with smaller maximum error at 50 Hz, indicating that the MHSC can facilitate tracking of such sawtooth signals.
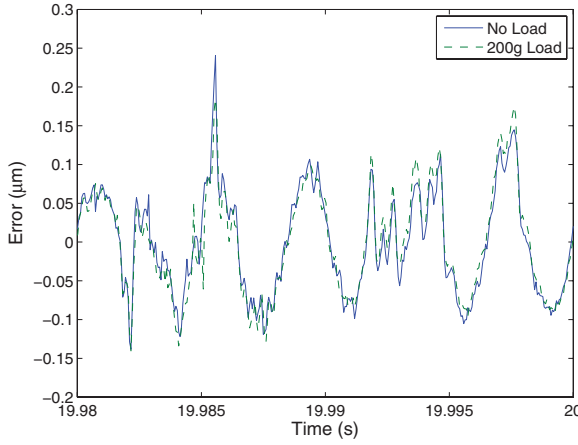
Fig. 12.   Tracking errors for a 50-Hz sinusoidal reference signal, for loaded and unloaded nanopositioner. A MHSC was used in both cases.

We also tested the performance of the proposed controller for references with more complex waveforms. Fig. 11(a) shows the experimental results for the proposed MHSC and ILC with a reference signal of

$$ y_r = 5 \sin \left(2\pi 5t - \frac{\pi}{2} \right) + 5 \sin \left(2\pi 15t + \frac{\pi}{2} \right) $$
$$ + 10 \sin \left(2\pi 25t - \frac{\pi}{2} \right). \tag{48} $$

Such an input excites more complex memory states for hysteresis, and is a useful test of the proposed controller's ability to compensate for hysteresis. The output–input hysteresis map in tracking this reference with MHSC is shown in Fig. 11(b), where we can clearly see multiple minor loops. The MHSC was designed to compensate for the reference signal alone, yielding a sixth-order servocompensator. The resulting mean tracking errors were 0.52% for the MHSC and 0.66% for ILC. Even though the reference is relatively slow, the advantage that ILC possesses over the MHSC at low frequencies for pure sinusoidal references has been reversed in this test by the MHSC. This evidences the effectiveness of the proposed controller at compensating hysteresis.

Finally, we investigated the robustness of the system's performance to loading conditions. To prevent damage to the nanopositioner, we limited our experiments to 40% (200 g) of the maximum load recommended by the manufacturer. ILC and MHSC (accommodating first three harmonics) were used for this paper. Table III shows the results for tracking a 50-Hz sinusoidal signal with a loaded nanopositioning stage, as well as the percent-change from the nominal results presented in Table I. The performance of the MHSC is nearly unchanged from the unloaded case, a point also readily visible in Fig. 12. Note that in Section IV-B, we were required to assume that the plant was perfectly known (i.e., $\Delta^* = 0$) to prove stability of the closed-loop system with hysteresis. However, the proposed controller with output feedback clearly enjoys robustness to changes in the system dynamics. The ILC controller, however, has suffered a notable drop in performance, with double-digit percentage drops in accuracy in the loaded case. However, due to ILC's better performance in the unloaded case, both

methods are very close in the raw performance. This result indicates that the MHSC's performance is significantly less tied to modeling accuracy than ILCs, since the net effect of a load is to deviate the plant from its nominal dynamics.

VI. CONCLUSION

In this paper, we have explored the potential of servocompensators in tracking periodic signals for systems with hysteresis. The control scheme combines a servocompensator with hysteresis inversion, and its performance in the presence of uncertainties in both hysteresis and dynamics was justified through rigorous analysis of the closed-loop system. We have experimentally demonstrated the high-frequency performance of this controller, and its robustness to loading conditions at frequencies compatible with existing SPM systems [49].

There are a few noteworthy trends seen in our experimental results. The most interesting trend, we observe is that the performance of the proposed method does not fall off with frequency as fast as the other control methods presented. For example, in the case of tracking sinusoids, the mean error increased only two-fold for the MHSC as the frequency increased from 5 to 200 Hz, as compared to 10- and 50-fold for ILC and P+I control, respectively. A very similar trend was seen in the sawtooth results shown in Table II. This shows the promise of MHSCs to facilitate high-frequency tracking in nanopositioners. We also note the high robustness of performance shown by the MHSC to loading conditions.

There are several potential directions for extending this paper. First, as mentioned in Section II, a few alternative stabilizing controllers can be used in conjunction with the servocompensator. For example, H_∞ loop-shaping techniques [48] can be used to reduce the effect of high-frequency harmonics like those seen in Fig. 9, and increase the tracking performance. For systems represented in observable canonical forms, high-gain observers [50] can readily facilitate the output feedback control.

Second, the design of the servocompensator requires the knowledge of the reference signal and the control parameters vary with the frequency of the reference. Adaptive servocompensators have already been proposed in [51] and others, and a worthwhile extension of our work would be to design a MHSC that can adapt to the frequency of the reference.

Finally, we note that in this paper we have used a finite-dimensional, classical or modified PI operator to model the hysteresis, where we have considered model uncertainties entering through the weight parameters. Conceivably, there will be a mismatch between the hysteresis nonlinearity in a physical system and what can be modeled with a classical/modified PI operator. While this type of modeling error can be reduced by increasing the numbers of play (and deadzone) elements in the PI model along with using sound practices in parameter identification, it is of interest to understand the impact of such modeling error on the tracking performance of our proposed control method. In particular, one could consider a small, unknown, hysteresis operator $\delta[v]$ that represents the difference between the actual hysteresis and the identified PI operator. Since the operator $\delta[\cdot]$ and the rest of the closed-loop

system form feedback connections, one interesting approach to potentially analyzing such systems would be to generalize the small gain theorem [50] to the hysteretic setting. Exploring these ideas will be a major undertaking, and it is beyond the scope of this paper.

References

[1] S. Devasia, E. Eleftheriou, and S. O. R. Moheimani, "A survey of control issues in nanopositioning," *IEEE Trans. Control Syst. Technol.*, vol. 15, no. 5, pp. 802–823, Sep. 2007.

[2] X. Tan and R. Iyer, "Modeling and control of hysteresis: Introduction to the special section," *IEEE Control Syst. Mag.*, vol. 29, no. 1, pp. 26–29, Feb. 2009.

[3] D. C. Jiles and D. L. Atherton, "Theory of ferromagnetic hysteresis," *J. Mag. Mater.*, vol. 61, nos. 1–2, pp. 48–60, 1986.

[4] A. Visintin, *Differential Models of Hysteresis*. New York: Springer-Verlag, 1994.

[5] J. Oh and D. Bernstein, "Semilinear Duhem model for rate-independent and rate-dependent hysteresis," *IEEE Trans. Autom. Control*, vol. 50, no. 5, pp. 631–645, May 2005.

[6] M. Krasnoselskii and A. Pokrovskii, *Systems with Hysteresis*. Berlin, Germany: Springer-Verlag, 1989.

[7] F. Preisach, "Ueber die magnetische Nachwirkung," *Annalen Der Phys.*, vol. 94, no. 5, pp. 277–302, 1935.

[8] I. Mayergoyz, *Mathematical Models of Hysteresis*. New York: Springer-Verlag, 1991.

[9] M. Brokate and J. Sprekels, *Hysteresis and Phase Transitions*. New York: Springer-Verlag, 1996.

[10] P. Krejci and V. Lovicar, "Continuity of hysteresis operators in Sobolev spaces," *Aplikace Mathematiky*, vol. 35, no. 1, pp. 60–66, 1990.

[11] R. C. Smith. (2005). *Smart Material Systems*, Society for Industrial and Applied Mathematics, Philadelphia, PA [Online]. Available: http://link.aip.org/link/doi/10.1137/1.9780898717471

[12] R. Iyer and X. Tan, "Control of hysteretic systems through inverse compensation: Inversion algorithms, adaptation, and embedded implementation," *IEEE Control Syst. Mag.*, vol. 29, no. 1, pp. 83–99, Feb. 2009.

[13] D. Croft, G. Shed, and S. Devasia, "Creep, hysteresis, and vibration compensation for piezoactuators: Atomic force microscopy application," *J. Dyn. Syst. Meas. Control*, vol. 123, no. 1, pp. 35–43, 2001.

[14] X. Chen, T. Hisayama, and C.-Y. Su, "Pseudo-inverse-based adaptive control for uncertain discrete time systems preceded by hysteresis," *Automatica*, vol. 45, no. 2, pp. 469–476, 2008.

[15] Y. Wu and Q. Zou, "Iterative control approach to compensate for both the hysteresis and the dynamics effects of piezo actuators," *IEEE Trans. Control Syst. Technol.*, vol. 15, no. 5, pp. 936–944, Sep. 2007.

[16] R. Gorbet, K. Morris, and D. Wang, "Passivity-based stability and control of hysteresis in smart actuators," *IEEE Trans. Control Syst. Technol.*, vol. 9, no. 1, pp. 5–16, Jan. 2001.

[17] G. Tao and P. V. Kokotovic, "Adaptive control of plants with unknown hystereses," *IEEE Trans. Autom. Control*, vol. 40, no. 2, pp. 200–212, Feb. 1995.

[18] J. Schfer and H. Janocha, "Compensation of hysteresis in solid-state actuators," *Sens. Actuat. A, Phys.*, vol. 49, nos. 1–2, pp. 97–102, 1995.

[19] A. Cavallo, C. Natale, S. Pirozzi, and C. Visone, "Effects of hysteresis compensation in feedback control systems," *IEEE Trans. Mag.*, vol. 39, no. 3, pp. 1389–1392, May 2003.

[20] C. Natale, F. Velardi, and C. Visone, "Identification and compensation of Preisach hysteresis models for magnetostrictive actuators," *Phys. B, Condensed Matter*, vol. 306, nos. 1–4, pp. 161–165, 2001.

[21] X. Tan and J. S. Baras, "Modeling and control of hysteresis in magnetostrictive actuators," *Automatica*, vol. 40, no. 9, pp. 1469–1480, 2004.

[22] P. Ge and M. Jouaneh, "Tracking control of a piezoceramic actuator," *IEEE Trans. Control Syst. Technol.*, vol. 4, no. 3, pp. 209–216, May 1996.

[23] R. Iyer, X. Tan, and P. Krishnaprasad, "Approximate inversion of the Preisach hysteresis operator with application to control of smart actuators," *IEEE Trans. Autom. Control*, vol. 50, no. 6, pp. 798–810, Jun. 2005.

[24] P. Krejci and K. Kuhnen, "Inverse control of systems with hysteresis and creep," *IEEE Proc. Control Theory Appl.*, vol. 148, no. 3, pp. 185–92, May 2001.

[25] K. Kuhnen, "Modeling, identification and compensation of complex hysteretic nonlinearities: A modified Prandtl–Ishlinskii approach," *Eur. J. Control*, vol. 9, no. 4, pp. 407–418, 2003.

[26] M. Al Janaideh, S. Rakheja, and C.-Y. Su, "An analytical generalized Prandtl–Ishlinskii model inversion for hysteresis compensation in micropositioning control," *IEEE/ASME Trans. Mechatron.*, vol. 16, no. 4, pp. 734–744, Aug. 2011.

[27] W. S. Galinaitis and R. C. Rogers, "Control of a hysteretic actuator using inverse hysteresis compensation," *Proc. SPIE*, vol. 3323, pp. 267–277, Jul. 1998.

[28] A. Hatch, R. Smith, T. De, and M. Salapaka, "Construction and experimental implementation of a model-based inverse filter to attenuate hysteresis in ferroelectric transducers," *IEEE Trans. Control Syst. Technol.*, vol. 14, no. 6, pp. 1058–1069, Nov. 2006.

[29] J. H. Ahrens, X. Tan, and H. K. Khalil, "Multirate sampled-data output feedback control with application to smart materialactuated systems," *IEEE Trans. Autom. Control*, vol. 54, no. 11, pp. 2518–2529, Nov. 2009.

[30] K. Kuhnen and H. Janocha, "Adaptive inverse control of piezoelectric actuators with hysteresis operators," in *Proc. Eur. Control Conf.*, 1999, pp. 973–976.

[31] X. Tan and J. S. Baras, "Adaptive identification and control of hysteresis in smart materials," *IEEE Trans. Autom. Control*, vol. 50, no. 6, pp. 827–839, Jun. 2005.

[32] X. Tan and H. K. Khalil, "Two-time-scale averaging of systems involving operators and its application to adaptive control of hysteretic systems," in *Proc. Amer. Control Conf.*, 2009, pp. 4476–4481.

[33] S. Bashash and N. Jalili, "Robust adaptive control of coupled parallel piezo-flexural nanopositioning stages," *IEEE/ASME Trans. Mechatron.*, vol. 14, no. 1, pp. 11–20, Feb. 2009.

[34] S. Salapaka, A. Sebastian, J. P. Cleveland, and M. V. Salapaka, "High bandwidth nano-positioner: A robust control approach," *Rev. Scientific Instrum.*, vol. 73, no. 9, pp. 3232–3241, 2002.

[35] C. Lee and S. M. Salapaka, "Fast robust nanopositioning: A linear-matrix-inequalities-based optimal control approach," *IEEE/ASME Trans. Mechatron.*, vol. 14, no. 4, pp. 414–422, Aug. 2009.

[36] Q. Zou, K. K. Leang, E. Sadoun, M. J. Reed, and S. Devasia, "Control issues in high-speed AFM for biological applications: Collagen imaging example," *Asian J. Control*, vol. 6, no. 2, pp. 164–178, 2004.

[37] J. Zhong and B. Yao, "Adaptive robust precision motion control of a piezoelectric positioning stage," *IEEE Trans. Control Syst. Technol.*, vol. 16, no. 5, pp. 1039–1046, Sep. 2008.

[38] J. Yi, S. Chang, and Y. Shen, "Disturbance-observer-based hysteresis compensation for piezoelectric actuators," *IEEE/ASME Trans. Mechatron.*, vol. 14, no. 4, pp. 454–462, Aug. 2009.

[39] E. J. Davison, "The robust control of a servomechanism problem for linear time-invariant multivariable systems," *IEEE Trans. Autom. Control*, vol. 21, no. 1, pp. 25–34, Feb. 1976.

[40] B. Francis and W. Wonham, "The internal model principle for linear multivariable regulators," *Appl. Math. Opt.*, vol. 2, no. 2, pp. 170–194, 1975.

[41] J. Shen, W. Jywe, and H. Chiang, "Precision tracking control of a piezoelectric-actuated system," in *Proc. 15th Mediterranean Conf. Control Autom.*, 2007, pp. 1–6.

[42] M. A. Janaideh, S. Rakheja, and C.-Y. Su, "A generalized Prandtl–Ishlinkskii model for characterizing the hysteresis and saturation nonlinearities of smart actuators," *Smart Mater. Struct.*, vol. 18, no. 4, pp. 045001-1–045001-9, 2009.

[43] L. Xie and I. Petersen, "Perfect regulation with cheap control for uncertain linear systems: A Riccati equation approach," *IET Control Theory Appl.*, vol. 2, no. 9, pp. 782–794, 2008.

[44] A. Esbrook, M. Guibord, X. Tan, and H. K. Khalil, "Control of systems with hysteresis via servocompensation and its application to nanopositioning," in *Proc. Amer. Control Conf.*, 2010, pp. 6531–6536.

[45] E. J. Davison, "The output control of linear time-invariant multivariable systems with unmeasurable arbitrary disturbances," *IEEE Trans. Autom. Control*, vol. 17, no. 5, pp. 621–630, Oct. 1972.

[46] B. A. Francis, "The linear multivariable regulator problem," *SIAM J. Control Opt.*, vol. 15, no. 3, pp. 486–505, 1977.

[47] A. V. Pokrovskii and M. Brokate, "Asymptotically stable oscillations in systems with hysteresis nonlinearities," *J. Different. Equations*, vol. 150, no. 1, pp. 98–123, 1998.

[48] K. Zhou, J. C. Doyle, and K. Glover, *Robust and Optimal Control*, 3rd ed. Englewood Cliffs, NJ: Prentice Hall, 1996.

[49] *The Aarhus SPM* [Online]. Available: http://www.specs.de/cms/upload/PDFs/SPECS Prospekte/Aarhus SPM Family Prospekt 2.pdf

[50] H. K. Khalil, *Nonlinear Systems*, 3rd ed. Englewood Cliffs, NJ: Prentice Hall, 2002.

[51] A. Serrani, A. Isidori, and L. Marconi, "Semiglobal nonlinear output regulation with adaptive internal model," *IEEE Trans. Autom. Control*, vol. 46, no. 8, pp. 1178–1194, Aug. 2001.

Alex Esbrook (S'10) received the B.S. degree in electrical engineering from Michigan State University, East Lansing, in 2008.

He has been a member of the Smart Microsystems Laboratory, Department of Electrical and Computer Engineering, Michigan State University, since May 2008. His current research interests include the control of systems with hysteresis, regulation theory, adaptive systems, automotive controls, and collaborative controls.

Mr. Esbrook was a recipient of an award for Best Session Presentation from the American Control Conference in 2010, and an honorable mention for the National Science Foundation Graduate Research Fellowship in 2009.
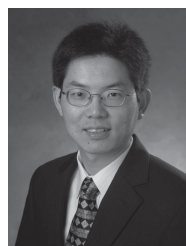
Xiaobo Tan (S'97–M'02–SM'11) received the B.Eng. and M.Eng. degrees in automatic control from Tsinghua University, Beijing, China, in 1995 and 1998, respectively, and the Ph.D. degree in electrical and computer engineering from the University of Maryland, College Park, in 2002.

He was a Research Associate with the Institute for Systems Research, University of Maryland, from September 2002 to July 2004. He joined the Faculty of the Department of Electrical and Computer Engineering, Michigan State University, (MSU), East Lansing, in 2004, where he is currently an Associate Professor. He is keen to integrate his research with educational and outreach activities, and currently leads an NSF-funded Research Experiences for Teachers (RET) Site on Bio-Inspired Technology and Systems (BITS) at MSU. His current research interests include modeling and control of smart materials, electroactive polymer sensors and actuators, biomimetic robotic fish, mobile sensing in aquatic environments, and collaborative control of autonomous systems.

Dr. Tan is an Associate Editor of *Automatica* and a Technical Editor of the IEEE/ASME TRANSACTIONS ON MECHATRONICS. He served as the Program Chair for the 15th International Conference on Advanced Robotics in 2011. He was a Guest Editor of the *IEEE Control Systems Magazine* for its February 2009 issue's Special Section on Modeling and Control of Hysteresis. He received the NSF CAREER Award in 2006, the 2008 ASME DSCD Best Mechatronics Paper Award with Yang Fang in 2009, and the Teacher-Scholar Award from MSU in 2010.

Hassan K. Khalil (F'89) received the B.S. and M.S. degrees in electrical engineering from Cairo University, Cairo, Egypt, in 1973 and 1975, respectively, and the Ph.D. degree from the University of Illinois at Urbana-Champaign, Urbana, in 1978, all in electrical engineering.

He has been with Michigan State University (MSU), East Lansing, since 1978, where he is currently a University Distinguished Professor of electrical and computer engineering. He has consulted for General Motors and Delco Products, and published several papers on singular perturbation methods and nonlinear control. He is the author of *Nonlinear Systems* (Macmillan 1992; Prentice Hall 1996 and 2002) and the co-author of *Singular Perturbation Methods in Control: Analysis and Design* (Academic Press 1986; SIAM 1999).

Dr. Khalil was named IFAC Fellow in 2007. He was a recipient of the IEEE-CSS George S. Axelby Outstanding Paper Award in 1989, the AACC Ragazzini Education Award in 2000, the IFAC Control Engineering Textbook Prize in 2002, the AACC O. Hugo Schuck Best Paper Award in 2004, and the AGEP Faculty Mentor of the Year Award in 2009. At MSU, he received the Teacher Scholar Award in 2003, the Withrow Distinguished Scholar Award in 1994, and the Distinguished Faculty Award in 1995. He served as an Associate Editor of the IEEE TRANSACTIONS ON AUTOMATIC CONTROL, *Automatica*, and *Neural Networks*, and as the Editor of *Automatica* for nonlinear systems and control. He was a Registration Chair of the 1984 CDC, Finance Chair of the 1987 ACC, Program Chair of the 1988 ACC, and General Chair of the 1994 ACC.